AIMS Energy, 8(4): 538–562.
DOI: 10.3934/energy.2020.4.538
Received: 22 April 2020
Accepted: 18 June 2020
Published: 28 June 2020

http://www.aimspress.com/journal/energy

Research article

Modeling of *Agave Salmiana* bagasse conversion by hydrothermal carbonization (HTC) for solid fuel combustion using surface response methodology

Diakaridia Sangare[1,2], Ayoub Missaoui[2], Stéphane Bostyn[2,3,*], Verónica Belandria[2,3], Mario Moscosa-Santillan[1] and Iskender Gökalp[2]

[1] Facultad de Ciencias Químicas Universidad Autónoma de San Luis Potosí Av. Dr. Nava # 6, Zona Universitaria San Luis Potosí, S.L.P., México 78210
[2] Institut de Combustion, Aérothermique, Réactivité, et Environnement (ICARE)-CNRS UPR3021, 1C avenue de la recherche scientifique 45071 Orléans Cedex 2, France
[3] Université d'Orléans, Institut Universitaire de Technologie, 16 rue d'Issoudun BP16724 45067 Orléans Cedex 2, France

* **Correspondence:** Email: stephane.bostyn@univ-orleans.fr; Tel: +33238255476; Fax: +33238696004.

Abstract: Hydrothermal carbonization (HTC) of *Agave Salmiana* bagasse was investigated to assess the potential of hydrochar as an energy resource. The effect of operating conditions on the mass yield and the energy quality of hydrochar was examined by varying the temperature and the holding time over the ranges of 180–250 °C (T) and 0–60 min (t), respectively. These parameters were screened using the response surface methodology through a Doehlert design. Performances of HTC were assessed on the basis of the hydrochar mass yield higher heating value ultimate and proximate analyses. In the studied domain, the modeling results indicated that the hydrochar mass yield varies between 45% and 86% and higher heating valuesfrom18 to 23 $MJ.kg^{-1}$, which is similar to that of peat. In addition, the volatile matter and fixed carbon fractions of hydrochars ranged from 54 to 80% and between 12 and 36%, respectively. Energy yield modeling indicated that the mass yield is the most influent parameter. The maximal energy yield value was obtained at 180 °C with time equal to 0 min. Globally, the evolution of H/C ratio is amplified for temperatures greater than 215 °C by increasing the holding time from 30 to 60 min. For O/C ratio the maximal variation is below these conditions. It is concluded that increased hydrothermal carbonization conditions favor dehydration reactions, while decarboxylation reactions are favored in mild HTC conditions. The combustion characteristics such as ignition peak and burnout temperatures were significantly modified for hydrochars. The model results

indicated that lowest ignition and peak temperature values are obtained at both low-temperature and low-holding time, and high-temperature and high-holding time zones. An increase in the burnout temperature was correlated with the increase of the fixed carbon content in hydrochars.

Keywords: *Agave Salmiana* bagasse; hydrothermal carbonization; hydrochar; solid fuel; modeling; response surface methodology; combustion characteristics

Nomenclature: HTC: Hydrothermal Carbonization; ASB: *Agave Salmiana* bagasse; HHV: Higher Heating Value (MJ/kg); MC: Moisture Content (%); VM: Volatile Matter (%); FC: Fixed Carbon (%); TGA: Thermo-Gravimetric Analysis (wt.%.); DTG: Derivative Thermo-gravimetric (wet.%/min); MY: Mass Yield (%); ED: Energy Densification ratio (-); EY: Energy Yield (%); RSM: Response Surface Methodology; Ti: Ignition Temperature (℃); Tm: Temperature at the maximum weight loss rate (℃); Tb: Burnout temperature (℃)

1. Introduction

Among renewable energy resources, biomass has emerged as a promising alternative to achieve upcoming energy targets and environmental challenges. Biomass contains less sulfur and nitrogen than fossil fuels, which reduces the emission of gaseous pollutants during their combustion [1–3]. In addition, in terms of CO_2 release, biomass is considered to have a carbon neutral balance [4]. The energy produced from biomass is the fourth largest energy resource behind oil, coal and natural gas. It represents about 10% of the world's primary energy production [5]. There is a wide range of biomass energy conversion technologies e.g. biological, chemical and thermochemical conversions (pyrolysis, gasification, combustion, torrefaction and hydrothermal carbonization). The optimal conversion depends on the nature of biomass and the type of energy desired. The biomass with a high moisture content (>50%) is suitable for hydrothermal carbonization, while biomass with a lower moisture content is more suitable for dry thermochemical processes [5]. Hydrothermal carbonization (HTC) is performed under the conditions of subcritical water between 180 ℃ and 250 ℃ and pressure between 1 and 4 MPa. Holding time of HTC treatment of lignocellulosic biomass is usually between a few minutes and several hours [6–9]. The nature of the biomass and the operating conditions (temperature, biomass to water weight ratio, particles size and holding time) affect the distribution and the composition of the final products [10]. The obtained hydrochar is a carbonaceous solid (55–74% carbon) [11] in which approximately 75–80% of the carbon containing in the feedstock is retained [7]. It is a lignite-like material characterized by high heating value (21.1–30.6 MJ/kg) [8,12,13]. The hydrochars produced during the HTC process are more hydrophobic than the raw biomass [5,14]. Hydrochar is more friable than the raw material which makes easier to produce pellets to feed gasifier or coal power plants [11], the hydrochar pellets can be densified at low compression pressure without an addition of a binder, also an additional heat treatment can improve the durability of hydrochar pellets [15]. The hydrochar was also used as nutrient sequestration or for amendment, but its performance seems to be very low compared to charcoal or pyrolysis coal [16]. Hydrochar can also be used as nanostructured carbon catalyst for the production of fine chemicals [13] and could be either activated as a low-cost adsorbent for water purification applications [17,18]; or as carbon material that increases a fuel cell's efficiency [19]]. The liquid from the HTC conversion

of the biomass is mainly composed of sugars (glucose, xylose, fructose, sucrose), organic acids (formic, acetic, lactic), phenolic compounds (phenol, cresol, catechol) and furfural derivatives while the obtained gas is mainly composed of CO_2 [7,8,20] The quality of HTC products depends of the biomass type and the operating process conditions. Distinct types of biomass have been investigated by the HTC process, tomato waste [21] sugarcane bagasse [22], corn cob [23] olive stone [6], olive pomace [5], etc. All these types of biomass are agro-industrial waste. In Mexico, one of the biggest agro-industrial waste generated is *Agave* bagasse.

There are almost 300 Agave species, all native to the American continent. Most of these species are found in México. The Agave plant has been used for 10,000 years to produce food, beverages and fibers [24]. In México, the production of distilled alcoholic beverages using agave is a tradition since the XVII century [25] Currently, these activities are also important in the Mexican economy. These beverages have different names, depending on the region of production; the most popular are tequila and mezcal. This last one is made from over 30 agave species, but the commonly used are agave *Angustifolia, karwinskii, Rodacantha, Potatorum and Agave Salmiana.* One of the mezcal-producing states is San Luis Potosi.

In San Luis Potosi, Mexico, about 720,000 liters/year of mezcal are produced [26], the agave species used is *Salmiana*. The production of mezcal begins with the harvest of agave plants that are more than 6 years old. In fact, the Agave heads rich on fructans named "piñas" are shaped in the form of pinecones. Heads undergo a solid/liquid extraction to extract fermentable sugars mainly composed of fructose and the solid residue is called bagasse [27]. The mezcal production process consists of 5 main steps: cooking, grinding, fermentation, distillation and maturation [28]. The process of obtaining these alcoholic drinks generates a sub-product called *Agave Salmiana* bagasse (ASB) of which 15 to 20 kg are produced on a wet basis (moisture content 70%), for each liter of mezcal produced [24,28]. In Mexico, it is estimated that the mezcal industry generates more than 141 tons of bagasse monthly [24]. In many of the mezcal-producing states, such as San Luis Potosi, this bagasse has no benefit for the mezcal producers. These wastes are given to the community for fodder. Sometimes they air dry it and burn it.

There are different studies on the valorization of bagasse. For example, Iñiguez-Covarrubias et al. [29] studied the use of bagasse as feed for ruminants, however this application was limited by the presence of lignin, the difficulty of animals to digest bagasse. The bagasse has been used to produce paper, the authors claim that this application is feasible, however a low mechanical resistance paper is found [30].

ASB was also studied as biosorbents precursor by Velazquez-Jimenez et al. [31]. The authors show that this application is efficient to remove Cd (II), Pb (II) and Zn (II) from water. However, these studies were not carried out in the practice; this waste has no practical application today. There are also studies on the use of bagasse as a renewable energy source, through the combustion of bagasse [24], this application is limited by the high moisture content (70%) of bagasse.

According to mezcal industry producers, the most energy-intensive process stage is the cooking, in this step, approximately 20 kWh (equivalent 72 MJ) of energy is used to produce one liter of mezcal. The amount of waste generated and the lack of uses, makes this sub-product can be explored as fuel allowing to save energy in the cooking step of agave processing. There are no scientific studies available in the literature to evaluate the potential of using the hydrochar obtained by HTC from ASB as an energy source. .This work focused on the conversion of *Agave Salmiana* bagasse by the HTC process. To understand the effects of the process parameters (temperature and holding time)

and the quality of the hydrochar produced, the characteristic factors for the use of hydrochar as an energy source have been studied. For this purpose, a Design of Experiments using the Doehlert method was applied for modelling the different factors and their characteristics using response surface methodology (RSM). In RSM, the visualization of the regression model can be obtained by surface response plots and 2D contour plots. These plots are useful to understand the nature of the response at different factor levels.

2. Materials and method

2.1. Biomass feedstock

The *Agave Salmiana* bagasse used in this study was collected from the distillery 'Ipiña' located in San Luis Potosi, Mexico. The ASB derives from *Agave Salmiana* plants commonly known as 'Maguey', an agro-waste material generated from the production of mezcal. The residue remaining after the juices have been extracted (bagasse pulp). In general, ASB has a moisture content of about 70%, ideal for hydrothermal carbonization process. Initially, ASB was air-dried, to reduce the moisture content, for storage and later transport from Mexico to France. It was subjected to natural open-air sun-drying, to a residual moisture content equal to 5% (dry bagasse), and used in experiments.

2.2. HTC experimental procedure

Details of the equipment and experimental procedure have been described in a previous study [5]. The HTC experiments were carried out in a 50 mL batch reactor (Top Industrie, France) made of a nickel-based alloy (Inconel 718). The HTC autoclave was heated in a furnace connected to a control panel to adjust and display the temperature. ASB and distilled water were introduced into the batch reactor at room temperature. Then, the residual air inside the reactor was removed by vacuum before starting the heating program at a specific pre-set temperature. When the pre-set temperature was reached, temperature was maintained during the selected holding time. At the end of this time, the reactor was cooled at room temperature using air circulation. The pressure (Pexp) and the final temperature (Texp) were noted. For each experiment, approximately 27 ± 0.001 g of distilled water was added to 3 ± 0.001 g of bagasse to obtain the biomass/water weight ratio equal to 1/9. It was demonstrated that the biomass/water weight ratio does not have any much influence on the hydrochar produced in the work of Missaoui et al. [5]. In fact, this ratio was chosen because of the fiber nature of the dried bagasse which swells with water contact. The experiment started with the heating phase where the autoclave was heated up to a pre-set temperature in the 180–250 °C range and maintained at this temperature for a fixed holding time up to 60 min.

2.3. Biomass and hydrochar characterization

2.3.1. Proximate, ultimate and component analyses

Proximate analysis was used for the assessment of moisture, volatile matter, fixed carbon, and ash content of biomass and hydrochar samples. The moisture content (MC) was obtained by a gravimetric method in accordance with the European standards (EN 14774-3: 2009: E). The ash

content, volatile matter (VM), and fixed carbon (FC) were determined using thermogravimetric (TG) proximate analysis technique. All experiments were performed on a simultaneous thermal Analyzer (STA) 449 F3 (Netzsch, Germany). After deducting the loss in mass due to moisture, the volatile matter was determined from the mass loss due to heating to 900 ℃ in N_2 ambience and isothermally holding for 7 min (EN 15148: 2009 E). The ash content was obtained from the remaining residue after combustion of the sample in air at 550 ℃ for biomass and 815 ℃ for hydrochar over a period of 2 h (EN 14775: 2009: E). Subsequently, the amount of fixed carbon was computed by summing the mass percent due to moisture content, volatile matter and ash, and subtracting the result from 100%, according to the following equation: FC (%) = 100 − [MC (%) + ash (%) + VM].

The standard deviation of triplicate runs is 1.4% for VM, 0.4% for ash, 1.0% for MC and 1.6% for FC. The elementals compositions were determined using a FLASH 2000 CHNS/O analyzer (Thermo Scientific), according to (CEN/TS 15104:2005). The high heating value (HHV) was determined using a bomb calorimeter (Parr 1261) and HHV values are given in MJ/kg on a dry basis.

Analyses of extractive, hemicellulose, cellulose and acid insoluble lignin fractions of raw ASB were performed according to the protocols described by Li et al. [32]The sample was dispersed in a toluene-ethanol solution to quantify extractives mass. The residue undergoes both basic and acid attacks to determine the hemicellulose and the acid insoluble lignin fractions, respectively. The cellulose content was determined by difference.

2.3.2. Characteristic combustion temperatures

The ignition and burning characteristics of the ASB residue and hydrochars were determined from thermogravimetric curves. A sample mass below 10 mg was used to minimize heat and mass transfer limitations. The experiments were carried out in air at a heating rate of 10 ℃/min and the samples were heated from 30 ℃ to 900 ℃. The Proteus analysis software (Netzsch, Germany) was used for smoothing, derivative calculation, extrapolating onset temperatures and peak maxima values. As in previous studies [33,34] a common TGA approach was employed to determine the ignition, maximum reaction rate and burnout temperature by identifying the relevant points of (TG-DTG) curves. Briefly, the ignition temperature (Ti) is associated with the temperature at which the fuel is likely to self-ignite, corresponding to the process onset temperature. The temperature related to the maximum rate of weight loss (dw/dt) max represents the temperature (Tm) at maximum combustion rate. Last (Tb), namely, burnout temperature, is considered as the stabilization temperature at which the combustion rate is less than 1 wt.%/min and the sample is completely oxidized [35]. Replicate measurements made for each sample indicated that the standard deviation for the extrapolated temperatures is within 2 ℃. In addition, the combustion reactivity [36,37]was estimated to evaluate fuel combustion performance, as follows: R_{index} = 100 x (dw/dt) max/Tm.

The temperature of autoignition was determined by using a method by temperature-controlled oven under oxygen atmosphere. For that, a TOC was used under a configuration for solid. For each experiment, 2 mg of solid is introduced into the furnace at the specific temperature. An oxygen flowrate of 170 mL min^{-1} was programmed and flowed into the furnace. The temperatures were decreased until no Gaussian peak of CO_2 was observed. The autoignition temperature was obtained from the first temperature where CO_2 peak was observed. The characteristic parameters in the present studies are given as mean values of runs carried out in triplicate.

2.3.3. Criteria to determine HTC performances

After each experiment, hydrochars were dried at 105 °C for 24 h in to determine the hydrochar mass yield (MY) and the energy yield (EY) as follows:

$$\text{Mass Yield} = \frac{\text{Mass}_{\text{Dry hydrochar}}}{\text{Mass}_{\text{Dry ASB}}} \quad (1)$$

$$\text{Energy densification ratio} = \frac{\text{HHV}_{\text{Dry hydrochar}}}{\text{HHV}_{\text{Dry ASB}}} \quad (2)$$

$$\text{Energy Yield} = \text{Mass Yield} * \text{Energy densification ratio} \quad (3)$$

$$\text{Hydrochar Energy (MJ/kg of dry hydrochar)} = \frac{\text{Energy yield}}{100}\text{HHV}_{\text{DryASB}} \quad (4)$$

For simplicity, the abbreviation: ASB-T-t will be used hereafter to denote the obtained hydrochars in accordance with the studied operating parameters, where T represents the HTC treatment temperature and t the holding time.

2.4. Modeling of the HTC conversion of ASB using a Doehlert experimental design

To model the HTC conversion of ASB, two variables are designated as important for the HTC process: temperature (T) and holding time (t). The particle size was not been investigated in order to work on raw material for avoiding no other operation of biomass transformation. Doehlert experimental design is selected because it needs fewer points to estimate the second-order terms Eq (5) is the used model for these two independent factors [38,39] The minimal number of experiments is 6 plus 3 in the center domain to estimate experimental errors. The experimental points are circumscribed into a sphere, and each factor is analyzed at different numbers of level depending on its influence on the response. In our case, the temperature factor is studied at 5 levels (between 180 °C and 250 °C) and the holding time at 3 levels (0, 30 and 60 min). Therefore, the choice of levels depends mainly on the ease of controlling the factor and its impact on the response. A typical quadratic model in Eq (1) was used to study the relationship between 2 parameters (temperature and holding time) and 10 responses (oxygen content, carbon content, MY, HHV, VM, FC, EY, Ti, Tm, Tb):

$$Y = b_0 + b_1X_1 + b_2X_2 + b_{11}X_1^2 + b_{12}X_1X_2 + b_{22}X_2^2 \quad (5)$$

where Y is the response, X_1 and X_2 are temperature and holding time, respectively.

The experimental conditions according to this design are given in Table 2. The experiment at the domain center (0, 0) is carried out in triplicate to calculate the experimental errors. The model consists of first-order terms (b_i), square terms (b_{ii}) and first-order interactions (b_{ij}). The estimation of the coefficients of the polynomial model (b_0, bi, b_{ii} and b_{ij} in Eq (5) is calculated using the least-square method by the use of Statgraphics Centurion XV Version Software (Sigma-Plus, Paris, France).

To appreciate, the quality of the models, the following parameters were calculated:

$$\text{Regression coefficient } (R^2): \ R^2 = \frac{SS_e}{SS_{tot}} \quad (6)$$

$$\text{Adjusted regression coefficient } (R^2_{adj}):\ R^2_{adj} = 1 - \frac{SS_{res}/(n-p)}{SS_{tot}/(n-1)} \frac{SS_{res}/(n-p)}{SS_{tot}/(n-1)} \quad (7)$$

$$\text{Predicted variation coefficient } (R^2_{pred}):\ R^2_{pred} = 1 - \frac{SS_{pre}}{SS_{tot}} \quad (8)$$

$$\text{with } SS_{pre} = PRESS = \sum_{i=1}^{n} e^2_{(i)} = \sum_{i=1}^{n} \left(\frac{e_i}{1-h_{ii}}\right)^2 \quad (9)$$

(PRESS means Predicted ResidualError Sum of Squares)

$$\text{Standard Error of estimate (SEE) :}\ SEE = \sqrt{\left(\frac{SS_{res}}{(n-p)}\right)} \quad (10)$$

SSe: sum of squares between calculated values (ŷi) and the mean value; SStot: sum of squares between experimental data and the mean; SSres: sum of the squares of model residuals; p: number of model coefficients; n: number of the experimental data; ei = (yi − ŷi), hii: ith diagonal element of the hat matrix H [40].

3. Results and discussion

3.1. Raw material characterization

In this study, the particles diameter used were between 100 μm to 1 mm. The results of proximate and ultimate analysis of untreated ASB are shown in Table 1. The moisture content (MC) of the raw ASB (5.0%) used in this work corresponds to the values found in the literature [24,41]. VM (77.9%) and FC (13.4%) fractions of raw ASB are also comparable to the values found by Liñán-Montes et al. [41]. The ASB has low ash content (3.8%), which is an advantage for combustion applications.

Ultimate analysis gives the weight percent of the elements C, H, O, N and S. Table 1 shows the elemental analysis of ASB. The quantity of oxygen is calculated by difference of 100% ASB. Its value is equal to 56.1%. Similar values were obtained for blue agave bagasse [41]. For higher contents of C and H, we observe higher energy content of the biomass [36]. The content of N and S is very important for the use of these materials in combustion. From an environmental viewpoint, The ASB can be an interesting fuel, since it has low N and S contents reduced the risk to produce NOx and SO_x emissions.

The results show that raw ASB contains 43.8% of hemicellulose, 40.7% of cellulose, 14.2% of lignin and 1.4% of extractives components. These values are similar to the blue agave bagasse fibers [42].

Ultimate analysis revealed that raw ASB has lower carbon percent (38.0%) in comparison to the oxygen percent (56.1%). ASB shows a HHV of 16.8 MJ/kg (comparable to the value of 16.3 MJ/kg reported by Liñán-Montes et al. [41]).

Table 1. Proximate, ultimate, extractive, hemicellulose, cellulose, lignin analysis, and heating values characteristics of ASB.

Proximate analysis (%)	
MC	5.0 ± 1.0
VM	77.9 ± 1.4
FC[a]	13.4 ± 1.6
Ash	3.8 ± 0.4
Ultimate analysis (%)	
C	38.0 ± 0.1
H	4.1 ± 0.1
N	0.6 ± 0.1
S	n.d
O[a]	56.1 ± 0.2
Extractible (%)	1.4 ± 0.0
Hemicellulose (%)	43.8 ± 0.4
Cellulose[a] (%)	40.7 ± 0.5
Lignin (%)	14.2 ± 0.1
HHV (MJ/kg)	16.8 ± 0.2

MC: moisture content; VM: volatile matter; FC: fixed carbon; n.d: not detectable (<0.1%); [a]: by difference.

3.2. Characteristics of hydrochars

3.2.1. Ultimate analyses

Results of ultimate analyses are given in Table 2. The evolution of hydrogen content is relatively stable around 5.3%. For the oxygen and carbon contents, their evolutions are more important. From data of Table 2, the effect of temperature and holding time on oxygen and carbon contents are shown in Figure 1a,b. For oxygen, its content decreases with an increase of parameters contrary to carbon content suggesting the carbonization of hydrochar.

The models that describe the evolution of the oxygen and carbon contents are the following: $O\ (\%) = 48.0 - 7.12X_1 - 5.28X_2 - 1.85X_1^2 + 1.85X_2^2$ and $C\ (\%) = 46.33 + 7.127X_1 + 5.11X_2 + 2.37\ X_1^2 - 1.733\ X_2^2$. These models were selected due to they give the best R^2_{adj} with a value of 90.6 % and 89.9% and SEE equal to 1.73% and 1.79% for oxygen and carbon, respectively. These models permit to trace the 2D contour plots represented in Figure 1c,d. The experimental errors are equal to 1%. The oxygen content decreased with increasing temperature while the carbon content of hydrochar increased with temperature. The carbon content was 36% for weak temperature and holding time and reached its maximum value (58%) for upper temperature and holding time in Figure 1c. However, the oxygen content had the same variation between 36% and 58% but in opposite direction in Figure 1d.

From these data, carbon retention rate (CR) can be calculated with the following equation:

$$CR_{hydrochar}\ (\%) = (1 \times 38 - 1 \times MY \times C_{hydrochar})/(1 \times 38). \quad (11)$$

Table 2. Fuel characteristics and chemical composition of hydrochars.

Run	X_1 (°C)	X_2 (min)	Proximate analysis (wt.%)				Ultimate analysis (wt.%)				HHV (MJ/kg)
			VM	FC	Moisture	Ash	C	H	O	N	
1	215 (0)	30 (0)	72.0	23.6	3.0	1.4	46 ± 1	5.5 ± 0.1	48 ± 1	0.27 ± 0.01	19.9
2	180 (−1)	30 (0)	73.7	17.3	4.5	4.2	43 ± 1	5.2 ± 0.1	52 ± 2	0.40 ± 0.02	18.1
3	250 (1)	30 (0)	59.4	33.9	2.5	4.2	54.4 ± 0.5	4.94 ± 0.04	40.3 ± 0.1	0.35 ± 0.01	23.2
4	197 (−0.5)	0 (−0.866)	81.3	13.3	4.7	0.7	36.4 ± 0.3	4.7 ± 0.1	58.0 ± 0.5	0.8 ± 0.1	18.5
5	215 (0)	30 (0)	74.7	20.8	3.0	1.4	46 ± 1	5.4 ± 0.1	49 ± 1	0.24 ± 0.05	20.6
6	232 (0.5)	60 (+0.866)	62.1	30.1	3.3	4.5	55.2 ± 0.5	5.3 ± 0.1	39.2 ± 0.4	0.33 ± 0.01	22.4
7	197 (−0.5)	60 (+0.866)	72.9	21.0	4.4	1.8	44.9 ± 0.2	5.4 ± 0.1	49.5 ± 0.2	0.22 ± 0.01	19.1
8	232 (0.5)	0 (−0.866)	71.1	20.8	3.3	4.9	46 ± 1	5.4 ± 0.1	49 ± 1	0.20 ± 0.01	19.1
9	215 (0)	30 (0)	74.2	20.8	3.1	2.0	47 ± 1	5.6 ± 0.1	47 ± 1	0.25 ± 0.02	20.1

The values of $CR_{hydrochar}$, for the extreme points of studied domain, are: 85% (−1; −0.866) and 61% (+1; +0.866). So $CR_{hydrochar}$ is superior to 61% indicating a carbon loss by 39% in all cases. The value of 85% is reached where the carbon content are minimum.

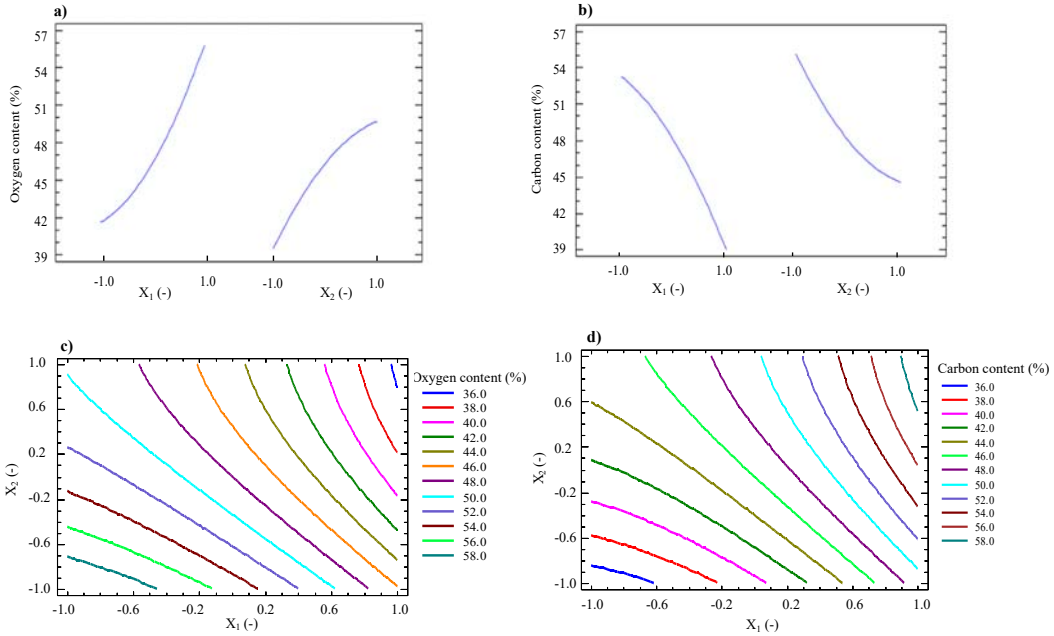

Figure 1. The main effect and 2D contour plots of temperature (X_1) and holding time (X_2) on the oxygen (a,c) and carbon (b,d).

The variation in the elemental composition of the raw ASB and hydrochars was analyzed via a Van-Krevelen diagram as illustrated in Figure 2. Van-Krevelen diagram provides general information about the quality and the nature of the solid fuel: lower atomic O/C and H/C ratios reduce the energy loss by fumes and steam released during combustion [43,44].

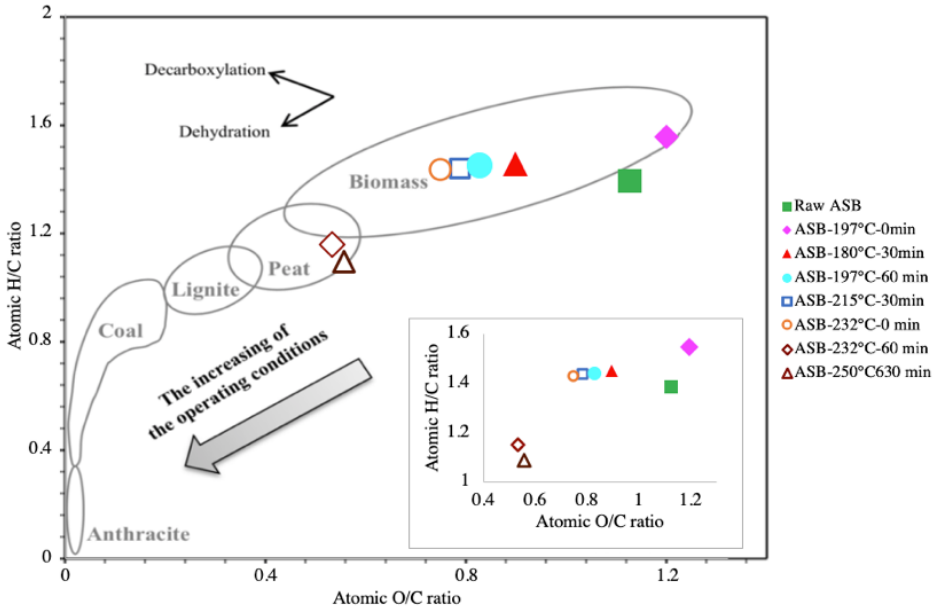

Figure 2. Van Krevelen diagram of raw ASB and hydrochars obtained at various holding times (0–60 min) and HTC treatment temperatures (180–250 °C) for an ASB/water weight ratio equal to 1/9.

The Van-Krevelen diagram (Figure 2) shows that the HTC treatment decreases the O/C and H/C atomic ratios of ASB resulting of oxygen and hydrogen loss during HTC process according to elemental analysis results. The ABS-232-60 decreases its H/C and O/C atomic ratios from 1.68 to 1.12 and 1.2 to 0.52 in comparison to ABS.

The evolution of the atomic O/C and H/C ratios allows the estimation of the degree of deoxygenation of the biomass by decarboxylation or by dehydration. The evolution of O/C and H/C shows that the decomposition of ASB was established by dehydration and decarboxylation reactions. But the treatment of ASB at extremes conditions (232 °C-60 min, and 250 °C-30 min) reveals the domination of dehydration reactions. The positions of most hydrochars, produced in this work, are inside the biomass domains indicating that the applied operating conditions were not sufficient to complete the decomposition of ASB by HTC reactions. In fact, the dehydration and decarboxylation trends became increasingly apparent at higher operating temperatures and longer holding time, indicating that the conversion of ASB during HTC process may be nearly complete at such long holding time. The position of hydrochars 232 °C-60 min and 250 °C-30 min in the region of the peat is in agreement with these explications. Furthermore, this general tendency is also due to the high oxygen and the low carbon contents of raw ASB.It is interesting to follow this ratio through the result of the DoE for representing the relation between the values of O/C and H/C as a function of temperature and holding time. The modeling responses of these ratios are shown in Figure 3.

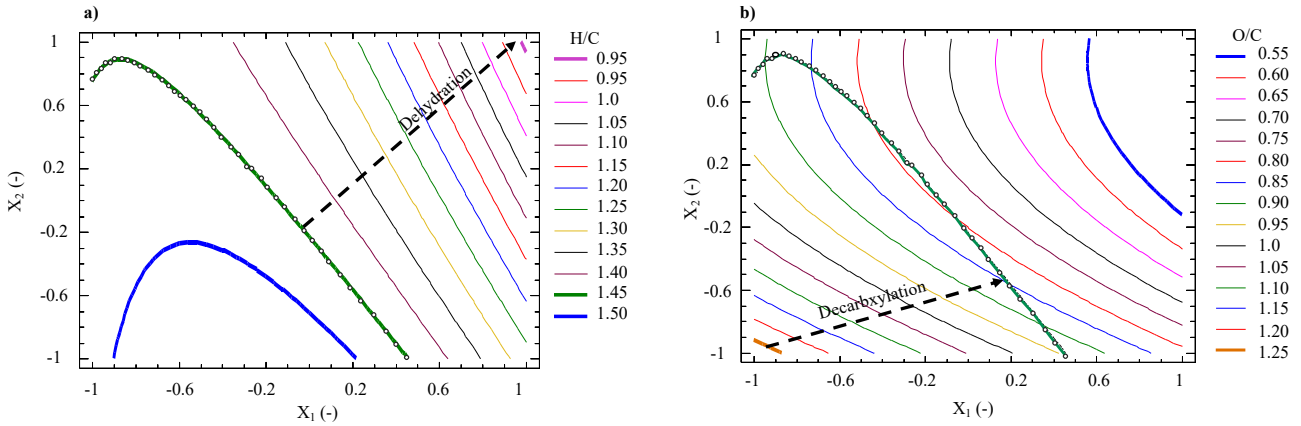

Figure 3. 2D contour plots showing the effects of temperature (X_1) and holding time (X_2) on: a) H/C, b) O/C.

The H/C and O/C models are given in the following equations:

$$H/C = 1.4257 - 0.1925X_1 - 0.1048X2 - 0.1546X_1^2 - 0.0867X_1X_2 \quad (12)$$

$$O/C = 0.7588 - 0.2322X_1 - 0.1832X_2 + 0.1060X_2^2 \quad (13)$$

The values of R^2_{adj} and SEE are: for H/C is (R^2_{adj} = 98.6%; SEE = 0.0174) and for O/C is (R^2_{adj} = 86.5%; SEE = 0.0714). It can be clearly noted that the evolution of O/C and H/C atomic ratios follow the paths of dehydration and decarboxylation reactions, the same trend as in the Van Krevelen diagram (Figure 2). As shown in the 2D contour plots (Figure 3) dehydration and decarboxylation are more intense as the HTC temperature (X_1) and holding time (X_2) increase, resulting in low O/C and H/C atomic ratios. In addition, the 2D contour plots for the H/C ratio (Figure 3a) reveal an area in which the parameters (X_1 and X_2) have a weak action on the process. This area is defined to the left of the line representing the H/C value equal to 1.45. This limit was represented in Figure 3b for the O/C ratio; the same trend was observed towards the right. It is well-known that towards lower values of H/C and O/C ratio, dehydration reactions are favored. Towards lower O/C values, the main reactions are decarboxylation. The model agrees with the Van Krevelen diagram. The most relevant finding is that the mathematical model defines the HTC process zones and the influence of parameters (X_1 and X_2) on the main HTC reactions dehydration and/or decarboxylation).

3.2.2. Proximate analyses and process characteristics

The results of these analyses are presented in Table 3 and Table 2. In all cases, it can be observed that the hydrochar produced presents less moisture content than the raw ASB (2.5–4.7% vs. 5%), The same results were observed by other works [9,45]. In fact, HTC removes the hydroxyl and carboxyl groups during the hydrolysis reactions of hemicellulose and cellulose, giving rise to a more hydrophobic residue than the raw material [5,9,46]. No significant variation in ash content between hydrochars and raw ASB was observed (0.7–4.5% vs. 3.8%), similar results were reported by Wiedner et al. [47] for HTC conversion of poplar wood and wheat straw.

Table 3. Doehlert matrix design responses for Temperature (X_1) and holding time (X_2) effects.

Run	X_1 (℃)	X_2 (min)	Responses					
			MY (%)	EY (%)	VM_{cal} (%)	FC_{cal} (%)	MY_{cal} (%)	HHVcal (MJ/kg)
1	215 (0)	30 (0)	65	77	73.6	21.7	65.6	20.2
2	180 (−1)	30 (0)	86	91	74.8	17.3	84.1	18.3
3	250 (+1)	30 (0)	45	62	58.2	33.9	47.1	23
4	197 (−0.5)	0 (−0.866)	82	90	80.3	12.9	84	18.3
5	215 (0)	30 (0)	66	81	73.6	21.7	65.6	20.2
6	232 (+0.5)	60 (+0.866)	52	69	63.3	29.7	50	22.6
7	197 (−0.5)	60 (+0.866)	70	80	71.6	21.4	72	18.9
8	232 (+0.5)	0 (−0.866)	71	81	72.1	21.2	69	19.1
9	215 (0)	30 (0)	66	79	73.6	21.7	65.6	20.2

From Table 3 the effects of temperature and holding time on MY, VM, HHV and FC are shown in Figure 4.

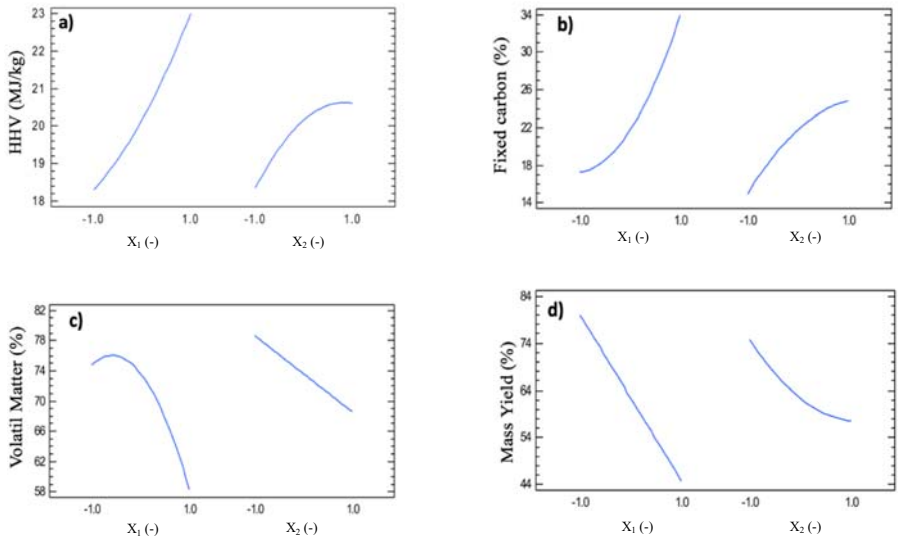

Figure 4. Main effects of temperature (X_1) and holding time (X_2) on a**)** HHV, b**)** fixed carbon, c**)** volatile matter, and d**)** mass yield of hydrocarbon produced.

The main effects are similar for MY and VM and for HHV and FC. For MY and VM, higher temperatures (X_1) and longer holding times (X_2) have negative effects. An increase of parameters (X_1 and X_2) decreases their values. while the HHV and FC values increase (Figure 4a,b) This same phenomenon was observed in biomass such as corn stover, rice hulls and switch grass in HTC [48] It is well known that an increase on these parameters (X_1 and X_2) decreases MY [49], but (Figure 4c) shows that it is mainly due to a loss of volatile matter. The HHV increased with HTC reaction temperature and can be related to an increase of fixed carbon content (Figure 4a,b). Hemicellulose and cellulose have a lower HHV and are less stable compared to lignin. When they are removed with increasing on the operating parameters, a higher proportion of lignin can be remained,

causing an increased HHV [48,50]. The increase in HHV may also be related to the proportion of benzene rings obtained by lignin decomposition [51,52].

The carbonization of biomass is also demonstrated by the fact that VM decreases when Temperature (X_1) and holding time (X_2) increases (Figure 4c) and through the evolution of carbon and oxygen percentages showed in Figure 1. Magdziarz et al. [53] reports that the main type of compounds mainly product in VM are aromatic, cyclic and aliphatic hydrocarbons, phenol and furan derivatives as well as oxygen compound as acids, ketones, aldehydes.

The performance of HTC was evaluated through MY, VM, HHV and FC for various X_1 and X_2 values by applying quadratic Eq 5). The influence of terms is shown on Pareto diagrams in Figure 5. In fact, from ANOVA, terms have been removed in view to obtain the maximal value of R^2_{adj} [38]. Regression coefficient of the model (R^2) gives the goodness of data fit, and R^2_{adj} takes into account the number of explanatory terms needed in the model. On Figure 5 a term is influent if its value is superior to the blue line ($p > 0.05$). In all cases, temperature and holding time are influent for each response. The values calculated with the following models (VMcal, FCcal, MYcal and HHVcal) are reported in Table 3.

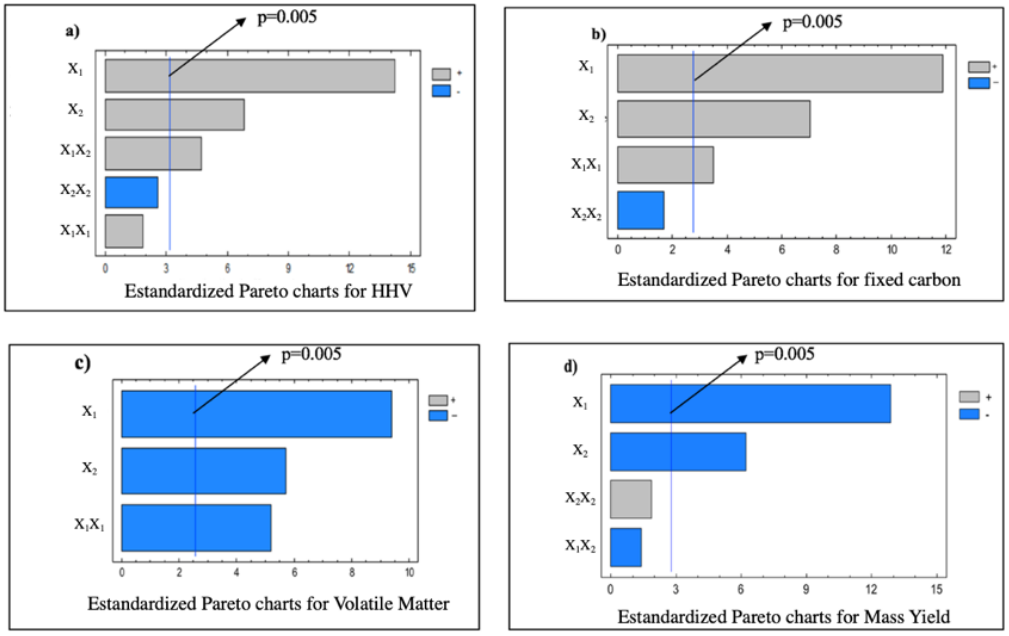

Figure 5. Pareto chart of standardized effects of Temperature (X_1) and holding time (X_2) on: a) HHV, b) fixed carbon, c) volatile matter and d) mass yield.

3.2.2.1. HHV Model

For hydrochar HHV, R^2_{adj} reaches a maximum with 5 coefficients and decreases afterwards. Therefore, the ideal combination of having the best fit without excess parameters requires five parameters corresponding to the following equation:

$$\text{HHV (MJ/kg)} = 20.2 + 2.35X_1 + 1.13X_2 + 0.45X_1^2 - 0.72X_2^2 + 1.59X_1X_2 \quad (14)$$

In this case, the value of the coefficient of determination (R^2) is 98% and R^2_{adj} is 94%. This value indicates that 6% of the variation is not explained by the model. The value of SEE is equal to 0.41% and experimental error equal to 0.5% meaning that model is well descriptive (R^2_{pred} = 0.61). This model gives a range of HHV between 18 and 24 MJ/kg (Figure 6a). These values are superior to the HHV of raw ASB. In this case, energy densification ratio value is superior to 1 and range between 1.07 to 1.42. Quadratic models were also reported in Román et al. [54].

3.2.2.2. Fixed Carbon Model

For the FC of hydrochar, R^2_{adj} reaches a maximum with 4 coefficients given following equation:

$$\text{FC}\ (\%) = 21.73 + 8.30X_1 + 4.91X_2 + 3.87X_1^2 - 1.87X_2^2 \quad (15)$$

With R^2 = 98%, R^2_{adj}=96%, SSE = 1.21% and R^2_{pred} = 0.95. For FC experimentations, experimental error is equal to 1.61% meanings that FC model is well descriptive but also predictive. FC model range is included between 12% and 36% (Figure 6b).

3.2.2.3. Mass Yield Model

For MY, model retained corresponds to the following equation:

$$\text{MY}\ (\%) = 65.60 - 18.50X_1 - 8.95X_2 + 4.20X_2^2 - 4.04X_1X_2 \quad (16)$$

With R^2 = 98%, R^2_{adj} = 96%, SSE = 2.49% and R^2_{pred} = 0.54. Experimental error is 0.58%. The value of R^2_{pred} indicates that this model would be expected to explain 54% of the variability in new data although R2adj is 96%. MY model range is included between 40% and 90% (Figure 6c).

3.2.2.4. Volatile Matter Model

For the VM of hydrochar, the adjusted R^2 reaches a maximum with 3 coefficients and decreases afterwards, therefore, the ideal combination of having the best fit without excess parameters requires three parameters corresponding to the following equation:

$$\text{VM}\ (\%) = 73.63 - 8.26X_1 - 5.02X_2 - 7.08X_1^2 \quad (17)$$

With R^2 = 97%, R^2_{adj} = 95%, SSE = 1.53%, experimental error is 1.44% and R^2_{pred} = 0.76. Model errors are slightly superior to experimental error. VM model range is included between 54% and 80% (Figure 6d).

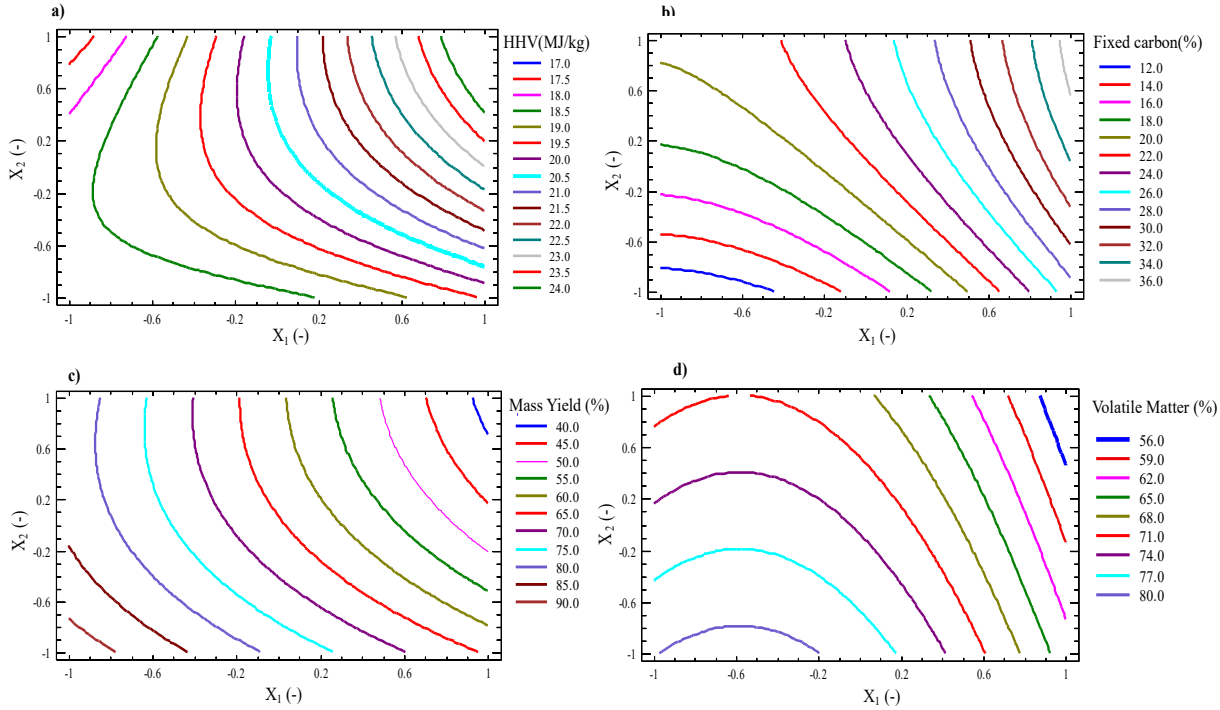

Figure 6. 2D contour plots showing the effects of temperature (X_1) and holding time (X_2) on: a) HHV, b) fixed carbon, c) volatile matter and d) mass yield.

3.2.2.5. HTC performance

From the results of HHV and MY, we can model the energy yield (EY) as a result of a compensation effect between the mass yield of the hydrochar and its energy quality (EY = MY × DE). Figure 7 shows the 2D contour graph of EY. The model equation is:

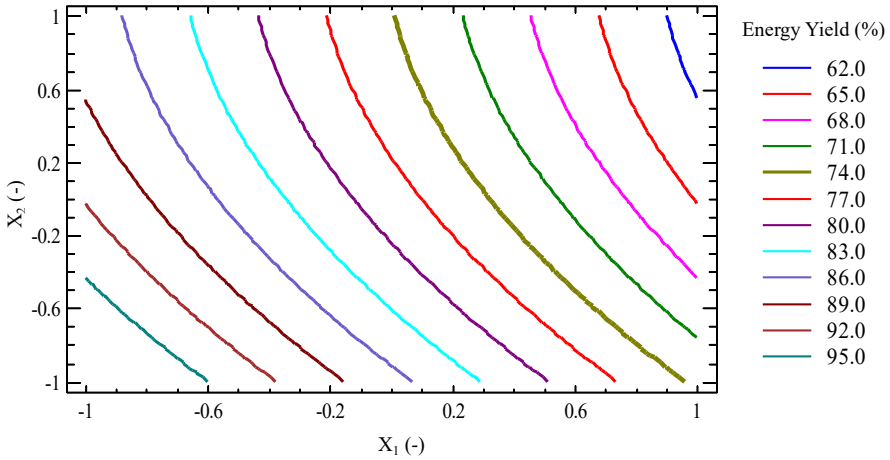

Figure 7. 2D contour plots showing the effects of temperature (X_1) and holding time (X_2) on energy yield.

$$EY\ (\%) = 78.33 - 13.48X1 - 6.38X2 + 2.20X_2^2 \quad (18)$$

With R^2 = 96%; R^2_{adj} = 90%; and SEE = 1,79%.

The optimal value is obtained for lower X_1 and X_2 following the MY tendency. Therefore, we can conclude that the MY is more influent in comparison to HHV. Furthermore, results show that the HTC treatment at 180 °C during 30 min treatment with an ASB/water weight ratio equal to 1/9 maximizes the energy yield (EY = 91%). The performance of energy yield of HTC conversion of ASB is presented in Table 3.

For a generalized energy balance, one liter of mezcal produced generates 15 kg of ASB with 70% moisture equivalent to 4.5 kg of ASB on a dry basis [24,28]. The energy yield value varies between 62 and 95% as shown in Figure 7. From Eq (4), it is estimated these hydrochars can produce between 46.87 MJ to 71.82MJ, which is equivalent to covering 65.10% to 99.75% of the energy required in the cooking step of the mezcal production process. However, a more detailed study of the overall energy balance of the HTC process would have to be carried out before a final conclusion could be drawn.

3.2.3. Thermal behavior (TG/DTG) of raw ASB and hydrochars

Typical curves of the thermogravimetric (TG) and derivative thermogravimetric (DTG) behavior of raw ASB and produced hydrochars, as a function of the studied parameters (temperature and holding time), are presented in Figure 8. The TG curves in Figure 8a show the mass loss percentage of samples over the range of temperature from 100 °C to 900 °C in nitrogen and heating rate (10 °C/min) conditions. The TG curves below 180 °C, which are related to moisture and volatiles releases, are almost similar for all samples. A mayor weight loss was observed at a temperature of 180–380 °C. In this range, the cellulose and hemicellulose decomposed leading to the formation of volatiles, primary char and gases [50]. After that, the rate of decomposition above 380 °C underwent a slow progress until 900 °C since the rest of the lignin or primary char was discomposed [55]. The TGA curve of hydrochar (ASB-250 °C-30min) suggests that the thermal stability increased with an increase in temperature.

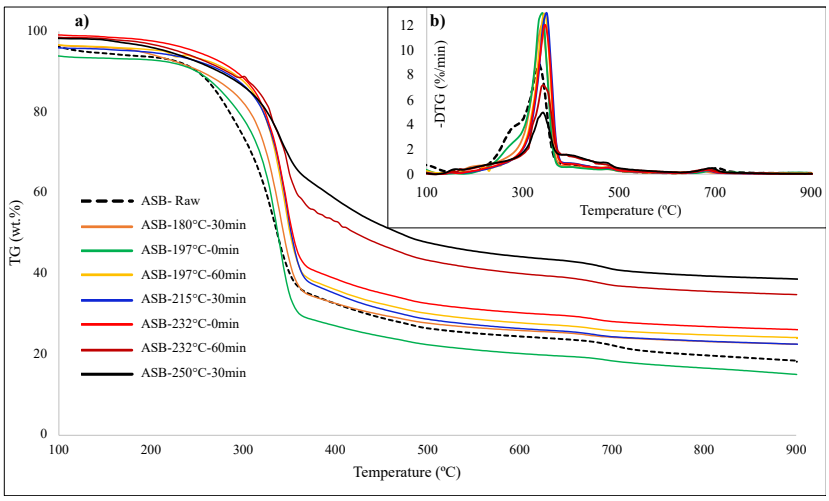

Figure 8. a) TG and b) DTG curves for raw ASB and hydrochars obtained at various holding times (0–60 min) and HTC treatment temperatures (180–250 °C).

The DTG curves presented in Figure 8b show that the raw ASB reaches its maximum mass loss at 340 ℃ which is attributed to cellulose decomposition. Hemicellulose can be attributed for temperatures lower than 300 ℃ [56,57]. The pyrolysis of lignin breaks down gradually over the broad temperature range of 275–500 ℃ [5,56].

The DTG curve is shifted from 340 ℃ for raw ASB to about 356 ℃. This shift can be explained by the formation of carbonaceous materials, such as 5-hydroxy-methyl-furfural which is a more stable compound than the initial feedstock [58,59]. For all hydrochars, degradation takes place over a wider temperature range, with mostly one sharp peak located between 280 ℃ and 380 ℃. This peak indicates that the largest mass loss is related to cellulose decomposition.

3.2.4. Combustion characteristics

A series of experiments were conducted to investigate the effect of the HTC operating conditions on the combustion behavior of hydrochars. The characteristic combustion parameters including T_i, T_m, T_b, $(dw/dt)_{max}$ and reactivity are summarized in Table 4. Above T_i, high decomposition rates take place, which are generally associated with the decomposition of hemicellulose and cellulose. An acceleration of the devolatilization rate $(dw/dt)_{max}$ is clearly noticed for hydrochars produced at 197 ℃ and 60 min ($(dw/dt)_{max}$ ~ 16.53). On the other hand, hydrochars produced at higher temperatures (232 ℃ and 250 ℃) with holding times of 30 and 60 minutes presented the lowest mass loss rate and R_{index} values compared to the other samples. This thermal behavior could be explained by the higher carbon content in these hydrochars (see Table 2) and may be linked to a more ordered carbonaceous structure, as described by Guizani et al. [36]. In addition, the corresponding reactivity increases for hydrochars obtained at 197 ℃ and 60 min, which may be due to the abundance of volatile matter and their slow process of combustion in the hydrochar. As assessed essentially by $(dw/dt)_{max}$, the higher the rate of combustion, the more reactive the hydrochar [37]. From the comparison of the $(dw/dt)_{max}$ and reactivity values of ASB ad derived hydrochars, hydrochars generally showed better fuel characteristics, except for the conditions identified above, e.g., higher temperatures and holding times corresponding to area with highest FC (Figure 6b).

Table 4. Characteristic temperatures and parameters on the combustion of raw ASB and hydrochars, at different HTC X_1 and X_2.

Sample	X_1 (℃)	X_2 (min)	Temperature (℃)			$(dw/dt)_{max}$ (%. min^{-1})	R_{index} (%. min^{-1}. ℃$^{-1}$)
			T_i	T_m	T_b		
ASB			270	326	479	10.06	3.09
1	215 (0)	30 (0)	301	329	527	15.70	4.78
2	180 (−1)	30 (0)	285	329	474	12.94	3.93
3	250 (+1)	30 (0)	279	323	638	5.21	1.61
4	197 (−0.5)	0 (−0.866)	296	323	490	14.49	4.49
5	215 (0)	30 (0)	300	328	530	12.13	3.68
6	232 (+0.5)	60 (+0.866)	283	315	591	5.04	1.60
7	197 (−0.5)	60 (+0.866)	304	329	495	16.53	5.03
8	232 (+0.5)	0 (−0.866)	301	331	500	14.62	4.42
9	215 (0)	30 (0)	302	328	517	14.68	4.48

T_i: ignition temperature; T_m: temperature at max. weight loss rate; T_b: burn out temperature; $(dw/dt)_{max}$: is the maximum observed reaction rate and R_{index}: is the reactivity index.

3.2.4.1. Ignition temperature

The ignition temperature (T_i) is the temperature that permits to promote a flame if the material is exposed to a source of inflammation. The T_i values obtained are superior to ASB one, thus indicating an increased difficulty of ignition with carbonization process. According to He et al. [60] this can be explained by the lower volatile matter in hydrochars compared to ASB.

The range of temperature ignition is between 279 ℃ and 304 ℃ for the experiment results. The model that give the best R^2_{adj} (94.8%) is represented by the following equation:

$$T_i(℃) = 300.87 - 4.67X_1 - 2.89X_2 - 18.93X_1^2 - 15.01X_1X_2 \quad (19)$$

The 2D contour plots (Figure 9a), shows the T_i values between 260 ℃ and 305 ℃. As it can be observed there is a large domain where the maximal value is possible and the lower values of Ti are for coordinates (+1; +0.866) or (−1; −0.866).

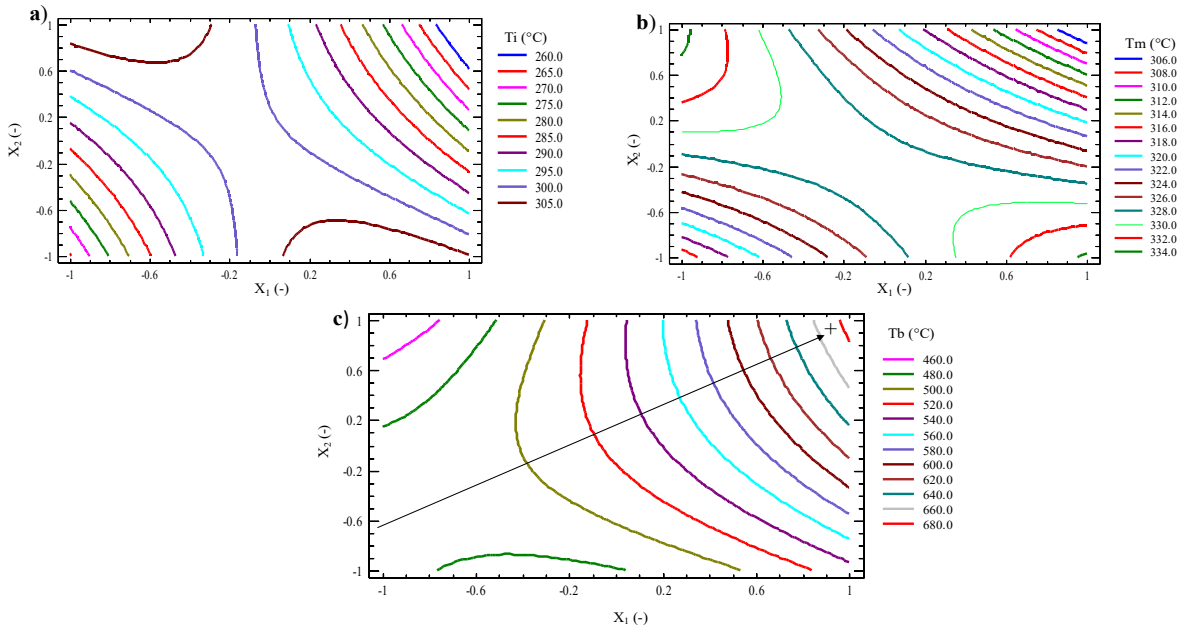

Figure 9. 2D contour plots showing the effects of temperature (X_1) and holding time (X_2) on: a) ignition temperature (T_i), b) the temperature at the point of the maximum weight loss rate (T_m) and c) the burnout temperature (T_b).

It is interesting to compare with the VM behavior because the ignition starts when there is enough flammable vapor to allow a combustion. We can observe where the VM content Figure 6d is maximal the T_i is minimal [60]. But the minimal T_i is also observed for high temperature and high treatment where VM content is minimal. That would mean that the onset devolatilization temperatures are equivalent.

To bring more argue on this temperature and to validate these results, we have determined the autoignition temperature by temperature-controlled oven under oxygen atmosphere. The results of five experiments selected in the studied domain are reported in Table 5.

Table 5. Autoignition temperatures of ASB and hydrochars, at different HTC X_1 and X_2.

Sample	$T_{autoignition}$ (°C)	T_i (°C)	$T_{autoignition} - T_i$ (°C)
ASB-232-60 (+0.5; +0.866)	241 ± 4	283	−42
ASB-232-0 (+0.5; −0.866)	325 ± 4	301	+24
ASB-215-30 (0; 0)	277 ± 4	301	−24
ASB-197-60 (−0.5; +0.866)	330 ± 4	304	+26
ASB-197-0 (−0.5; −0.866)	310 ± 4	296	+14
Raw material	310 ± 4		

The results of $T_{autoignition}$ determined (Table 5) show that the minimal value is for sample ASB-232-60 corresponding to the minimal T_i value also, it is quite interesting to see the similar values for raw material and ASB-197-0. This can be explained by the fact that process has not modified ASB-197-0 enough to show a difference in $T_{autoignition}$. Their visual aspect was similar. The ASB-197-0 sample kept the fibrous aspect. Besides, for ASB-232-0 and ASB-197-60 and ASB-197-0,

$T_{autoignition}$ values are greater than T_i. This can be explained by volatile compounds that have a superior $T_{autoignition}$ than T_i. Above T_i, high decomposition rates take place, mainly related to the decomposition of hemicellulose and cellulose.

3.2.4.2. Temperature at the maximum weight loss rate

Tm corresponds to the fastest mass loss when the temperature acts. The T_m profile of 2D contour plots (Figure 9b) has a similar shape than the Ti one. To build the 2D contour plots, the model retained has the following equation:

$$T_m(°C) = 328.33 - 3.0X_1 - 2.87X_2 - 2.33X_1^2 - 4.33X_2^2 - 12.70X_1X_2 \quad (20)$$

The model gives a R^2_{adj} value of 99.11%. The minimum value equal to 306 °C is for (+1; +0.866) experiment and corresponds also to the experiment that has the maximal FC content. The maximal values are obtained for the (−1; +0.866) and (−1; −0.866) experiments corresponding to the domain where there are not the maximum VM content or FC content.

3.2.4.3. Burnout temperature

The 2D contour plots are shown in Figure 9c It is obtained with the following equation with R^2_{adj} = 92.2%:

$$T_b(°C) = 524.68 + 72.33X_1 + 27.71X_2 + 31.33X_1^2 - 18.00X_2^2 + 49.65X_1X_2 \quad (21)$$

The maximal value equal to 680 °C is for (+1; +0.866) experiment. The evolution of Tb follows the FC content evolution. More the content of FC is important more the Tb is also important due to an increasing of thermal stability of hydrochar.

4. Conclusions

Modeling of ASB conversion by HTC at different process conditions using surface response methodology (RSM) has been investigated. The HHV modeling gives a maximal value equal to 24.0 MJ/kg against 16.8 MJ/kg for raw ASB. It is also shown that the energy yield provided by the hydrochar could compensate the energy required in the cooking step of the mezcal production process. However, a more detailed study of the overall energy balance of the HTC process would have to be carried out before a final conclusion can be drawn.

Models describing the behavior of HHV, MY, FC, VM, T_i, T_m and Tb as function of the process conditions (temperature, holding time) were obtained. These models could be useful to select the optimal experimental conditions to produce hydrochars with a high energy content for their use as fuel. RSM of H/C and O/C showed that increased HTC conditions favored dehydration reactions, while decarboxylation reactions were favored in mild HTC conditions. The proposed 2D contour plots bring useful supplementary information to Van Krevelen diagram

Moreover, the investigation of combustion parameters provided a better understanding of the thermal behavior of biomass and hydrochars. The lowest autoignition temperature resulted equal to 241 °C for hydrochars against 310 °C for raw bagasse. In general, it was observed that the minimum Ti and Tm values occur for a minimal and maximal degree of devolatilization. In addition,

lower temperatures and holding times promote a maximum volatile matter release for all hydrochars. Furthermore, an increase in the burnout temperature was related to an increase of the fixed carbon content.

Acknowledgments

This research work was conducted under VERA-P2 project. We acknowledge the Région Centre-Val de Loire and the CNRS for financial support. This work is also supported by the French Goverment's Investissement d'Avenir program: Laboratoire d'Excellence CAPRYSSES (Grant No. ANR-11-LABX-0006-01). We also thank Florine Pasquet for technical assistance with experiments.

Conflict of interest

No conflict of interest.

Supplementary

Graphic abstract

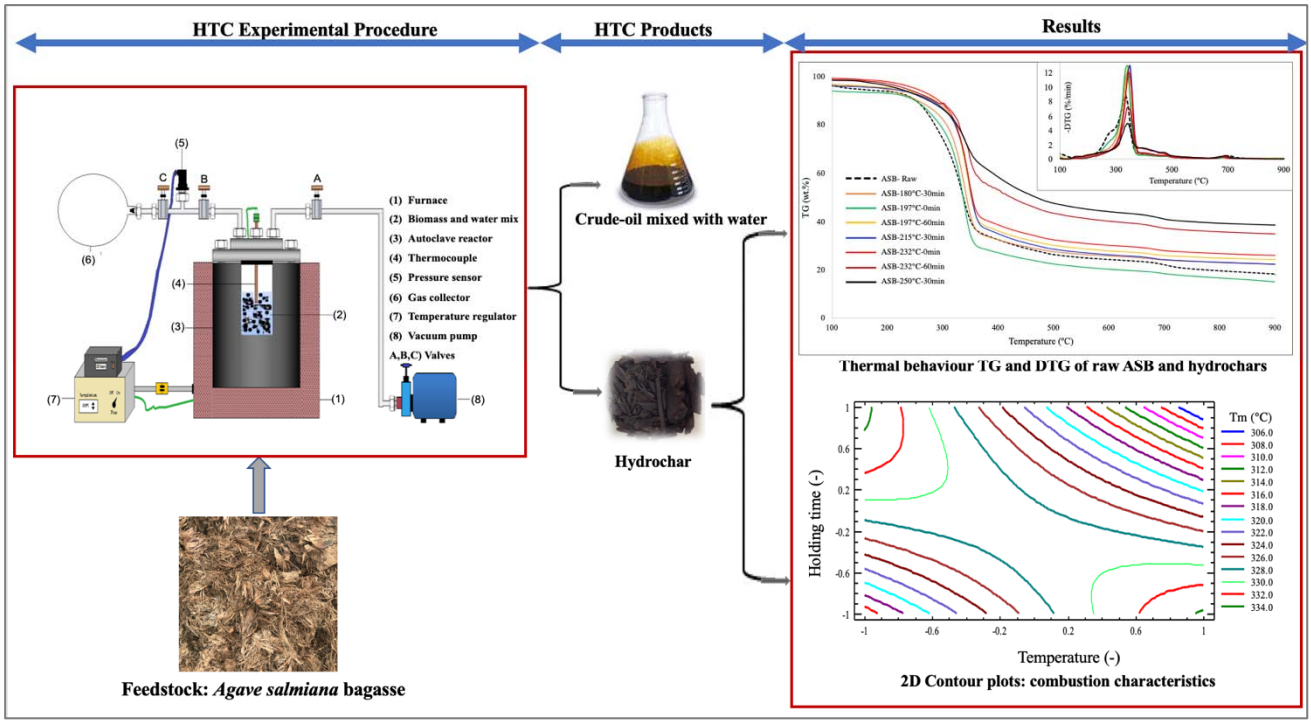

References

1. Balat M, Balat M, Kırtay E, et al. (2009) Main routes for the thermo-conversion of biomass into fuels and chemicals. Part 1: Pyrolysis systems. *Energy Convers Manage* 50: 3147–3157.
2. McKendry P (2002) Energy production from biomass (part 1): Overview of biomass. *Bioresour Technol* 83: 37–46.

3. Vassilev SV, Baxter D, Andersen LK, et al. (2010) An overview of the chemical composition of biomass. *Fuel* 89: 913–933.
4. Mujtaba IM, Srinivasan R, Elbashir N (2017) The water-food-energy nexus: processes, technologies, and challenges: CRC Press.
5. Missaoui A, Bostyn S, Belandria V, et al. (2017) Hydrothermal carbonization of dried olive pomace: Energy potential and process performances. *J Anal Appl Pyrolysis* 128: 281–290.
6. Álvarez-Murillo A, Román S, Ledesma B, et al. (2015) Study of variables in energy densification of olive stone by hydrothermal carbonization. *J Anal Appl Pyrolysis* 113: 307–314.
7. Benavente V, Calabuig E, and Fullana A (2015) Upgrading of moist agro-industrial wastes by hydrothermal carbonization. *J Anal Appl Pyrolysis* 113: 89–98.
8. Hoekman SK, Broch A, Robbins C (2011) Hydrothermal carbonization (HTC) of lignocellulosic biomass. *Energy Fuels* 25: 1802–1810.
9. Yan W, Acharjee TC, Coronella CJ, et al. (2009) Thermal pretreatment of lignocellulosic biomass. *Environ Prog Sustainable Energy: Am Inst Chem Eng* 28: 435–440.
10. Tekin K, Karagöz S, Bektaş S (2014) A review of hydrothermal biomass processing. *Renewable Sustainable Energy Rev* 40: 673–687.
11. Libra JA, Ro KS, Kammann C, et al. (2011) Hydrothermal carbonization of biomass residuals: A comparative review of the chemistry, processes and applications of wet and dry pyrolysis. *Biofuels* 2: 71–106.
12. Hitzl M, Corma A, Pomares F, et al. (2015) The hydrothermal carbonization (HTC) plant as a decentral biorefinery for wet biomass. *Catal Today* 257: 154–159.
13. Xiao LP, Shi ZJ, Xu F, et al. (2012) Hydrothermal carbonization of lignocellulosic biomass. *Bioresour Technol* 118: 619–623.
14. Acharjee TC, Coronella CJ, Vasquez VR (2011) Effect of thermal pretreatment on equilibrium moisture content of lignocellulosic biomass. *Bioresour Technol* 102: 4849–4854.
15. Surup GR, Leahy JJ, Timko MT, et al. (2020) Hydrothermal carbonization of olive wastes to produce renewable, binder-free pellets for use as metallurgical reducing agents. *Renewable Energy*.
16. Reza MT, Nover J, Wirth B, et al. (2018) Hydrothermal carbonization of glucose in saline solution: sequestration of nutrients on carbonaceous materials. 4: 173, 2016.
17. Kumar S, Loganathan VA, Gupta RB, et al. (2011) An assessment of U (VI) removal from groundwater using biochar produced from hydrothermal carbonization. *J Environ Manage* 92: 2504–2512.
18. Regmi P, Moscoso JLG, Kumar S, et al. (2012) Removal of copper and cadmium from aqueous solution using switchgrass biochar produced via hydrothermal carbonization process. *J Environ Manage* 109: 61–69.
19. Hu B, Wang K, Wu L, et al. (2010) Engineering carbon materials from the hydrothermal carbonization process of biomass. *Adv Mater* 22: 813–828.
20. Reza MT, Rottler E, Herklotz L, et al. (2015) Hydrothermal carbonization (HTC) of wheat straw: Influence of feedwater pH prepared by acetic acid and potassium hydroxide. *Bioresour Technol* 182: 336–344.
21. Sabio E, Álvarez-Murillo A, Román S, et al. (2016) Conversion of tomato-peel waste into solid fuel by hydrothermal carbonization: Influence of the processing variables. *Waste Manage* 47: 122–132.

22. Chen WH, Ye SC, Sheen HK (2012) Hydrothermal carbonization of sugarcane bagasse via wet torrefaction in association with microwave heating. *Bioresour Technol* 118: 195–203.
23. Zhang L, Liu S, Wang B, et al. (2015) Effect of residence time on hydrothermal carbonization of corn cob residual. *BioResources* 10: 3979–3986.
24. Chávez-Guerrero L, Hinojosa M (2010) Bagasse from the mezcal industry as an alternative renewable energy produced in arid lands. *Fuel* 89: 4049–4052.
25. Marín PC-G, Saavedra AL, Eguiarte LE, et al. (2007) En lo ancestral hay futuro: del tequila, los mezcales y otros agaves. *Revista de la Universidad de Yucatán, NÚMEROS*. 245: 246.
26. Gonzales B (2005) Aprovechamiento del bagazo del maguey verde (Agave salmiana) de la agroindustria del mezcal en San Luis Potosı para la producción de hongo ostra (Pleurotus ostreatus). Ph Thesis. Instituto Potosino de Investigación Cientıfica y Tecnologıca AC. México, Tesis de Maestría en Ciencias Ambientales.
27. Michel-Cuello C, Juárez-Flores BI, Aguirre-Rivera JR, et al. (2008) Quantitative characterization of nonstructural carbohydrates of mezcal Agave (Agave salmiana Otto ex Salm-Dick). *J Agric Food Chem* 56: 5753–5757.
28. Chávez Guerrero L (2010) Uso de bagazo de la industria mezcalera como materia prima para generar energía. *Ingenierías* 13: 8–16.
29. Iñiguez-Covarrubias G, Lange SE, Rowell RM (2001) Utilization of byproducts from the tequila industry: part 1: agave bagasse as a raw material for animal feeding and fiberboard production. *Bioresour Technol* 77: 25–32.
30. Idarraga G, Ramos J, Zuñiga V, et al. (1999) Pulp and paper from blue agave waste from tequila production. *J Agric Food Chem* 47: 4450–4455.
31. Velazquez-Jimenez LH, Pavlick A, Rangel-Mendez JR (2013) Chemical characterization of raw and treated agave bagasse and its potential as adsorbent of metal cations from water. *Ind Crops Prod* 43: 200–206.
32. Li S, Xu S, Liu S, et al. (2004) Fast pyrolysis of biomass in free-fall reactor for hydrogen-rich gas. *Fuel Process Technol* 85: 1201–1211.
33. Li X-g, Ma B-g, Xu L, et al. (2006) Thermogravimetric analysis of the co-combustion of the blends with high ash coal and waste tyres. *Thermochim Acta* 441: 79–83.
34. Wang C, Wang F, Yang Q, et al. (2009) Thermogravimetric studies of the behavior of wheat straw with added coal during combustion. *Biomass Bioenergy* 33: 50–56.
35. Peng C, Zhai Y, Zhu Y, et al. (2016) Production of char from sewage sludge employing hydrothermal carbonization: char properties, combustion behavior and thermal characteristics. *Fuel* 176: 110–118.
36. Guizani C, Jeguirim M, Valin S, et al. (2017) Biomass chars: The effects of pyrolysis conditions on their morphology, structure, chemical properties and reactivity. *Energies* 10: 796.
37. Pala M, Kantarli IC, Buyukisik HB, et al. (2014) Hydrothermal carbonization and torrefaction of grape pomace: A comparative evaluation. *Bioresour Technol* 161: 255–262.
38. Chartier A, Beaumesnil M, de Oliveira AL, et al. (2013) Optimization of the isolation and quantitation of kahweol and cafestol in green coffee oil. *Talanta* 117: 102–111.
39. Ferreira SL, Queiroz AS, Fernandes MS, et al. (2002) Application of factorial designs and Doehlert matrix in optimization of experimental variables associated with the preconcentration and determination of vanadium and copper in seawater by inductively coupled plasma optical emission spectrometry. *Spectrochim Acta Part B* 57: 1939–1950.

40. Mäkelä M, Benavente V, Fullana A (2015) Hydrothermal carbonization of lignocellulosic biomass: effect of process conditions on hydrochar properties. *Appl Energy* 155: 576–584.
41. Linan-Montes A, De la Parra-Arciniega S, Garza-González M, et al. (2014) Characterization and thermal analysis of agave bagasse and malt spent grain. *J Therm Anal Calorim* 115: 751–758.
42. Flores-Sahagun TH, Dos Santos LP, Dos Santos J, et al. (2013) Characterization of blue agave bagasse fibers of Mexico. *Composites Part A: Appl Sci Manuf* 45: 153–161.
43. Kambo HS, Dutta A (2015) A comparative review of biochar and hydrochar in terms of production, physico-chemical properties and applications. *Renewable Sustainable Energy Rev* 45: 359–378.
44. Liu Z, Quek A, Hoekman SK, et al. (2013) Production of solid biochar fuel from waste biomass by hydrothermal carbonization. *Fuel* 103: 943–949.
45. Stirling RJ, Snape CE, Meredith W (2018) The impact of hydrothermal carbonisation on the char reactivity of biomass. *Fuel Process Technol* 177: 152–158.
46. Funke A, Ziegler F (2010) Hydrothermal carbonization of biomass: a summary and discussion of chemical mechanisms for process engineering. *Biofuels, Bioprod Biorefin* 4: 160–177.
47. Wiedner K, Naisse C, Rumpel C, et al. (2013) Chemical modification of biomass residues during hydrothermal carbonization–What makes the difference, temperature or feedstock? *Org Geochem* 54: 91–100.
48. Lynam JG, Reza MT, Yan W, et al. (2015) Hydrothermal carbonization of various lignocellulosic biomass. *Biomass Convers Biorefin* 5: 173–181.
49. Wang T, Zhai Y, Zhu Y, et al. (2018) A review of the hydrothermal carbonization of biomass waste for hydrochar formation: Process conditions, fundamentals, and physicochemical properties. *Renewable Sustainable Energy Rev* 90: 223-247.
50. Demirbas A (2004) Effects of temperature and particle size on bio-char yield from pyrolysis of agricultural residues. *J Anal Appl Pyrolysis* 72: 243–248.
51. Collard F-X, Blin J (2014) A review on pyrolysis of biomass constituents: Mechanisms and composition of the products obtained from the conversion of cellulose, hemicelluloses and lignin. *Renewable Sustainable Energy Rev* 38: 594–608.
52. Kang S, Li X, Fan J, et al. (2012) Characterization of hydrochars produced by hydrothermal carbonization of lignin, cellulose, D-xylose, and wood meal. *Ind Eng Chem Res* 51: 9023–9031.
53. Magdziarz A, Wilk M, Wądrzyk M (2020) Pyrolysis of hydrochar derived from biomass–Experimental investigation. *Fuel* 267: 117246.
54. Román S, Libra J, Berge N, et al. (2018) Hydrothermal carbonization: modeling, final properties design and applications: a review. *Energies* 11: 216.
55. Wongsiriamnuay T, Tippayawong N (2010) Non-isothermal pyrolysis characteristics of giant sensitive plants using thermogravimetric analysis. *Bioresour Technol* 101: 5638–5644.
56. Lee Y, Park J, Ryu C, et al. (2013) Comparison of biochar properties from biomass residues produced by slow pyrolysis at 500 C. *Bioresour Technol* 148: 196–201.
57. Wang J, Shen B, Kang D, et al. (2019) Investigate the interactions between biomass components during pyrolysis using in-situ DRIFTS and TGA. *Chem Eng Sci* 195: 767–776.
58. Basso D, Patuzzi F, Castello D, et al. (2016) Agro-industrial waste to solid biofuel through hydrothermal carbonization. *Waste Manage* 47: 114–121.
59. Sevilla M, Fuertes AB (2009) The production of carbon materials by hydrothermal carbonization of cellulose. *Carbon* 47: 2281–2289.

60. He C, Giannis A, Wang JY (2013) Conversion of sewage sludge to clean solid fuel using hydrothermal carbonization: hydrochar fuel characteristics and combustion behavior. *Appl Energy* 111: 257–266.